Composites: Part B 68 (2015) 246–258

Contents lists available at ScienceDirect

Composites: Part B

journal homepage: www.elsevier.com/locate/compositesb

Mechanical behaviour of ultra-high-performance short-fibre-reinforced concrete beams with internal fibre reinforced polymer bars

E. Ferrier [a,*], L. Michel [a], B. Zuber [b], G. Chanvillard [b]

[a] LGCIE Site Bohr, Université Claude Bernard Lyon I, Domaine Scientifique de la DOUA, 82 Boulevard Niels Bohr, 69622 Villeurbanne Cedex, France
[b] Lafarge, LCR, Saint Quentin Fallavier, France

ARTICLE INFO

Article history:
Received 10 December 2013
Received in revised form 15 July 2014
Accepted 1 August 2014
Available online 16 September 2014

Keywords:
A. Carbon fibre
B. Mechanical properties
B. Stress transfer
C. Analytical modelling
D. Mechanical testing

ABSTRACT

The primary objective of this research was to develop a new type of high-performance lightweight beam providing better performance than conventional beams made of timber, steel or reinforced concrete (RC) by casting fibre-reinforced polymer (FRP) reinforcing bars (rebars) in ultra-high-performance concrete with short fibre reinforcement (UHPC–SFR). This new type of beam was developed to be lightweight, have high compressive and tensile strength, be able to sustain large bending moments and be resistant to shear. The main objective was to verify the mechanical behaviour of the beams and compare it with typical RC beam behaviour. For this purpose, an experimental program was designed to identify the failure modes and bending behaviour. The results indicate that the behaviour of such RC beams can be compared to typical RC beam behaviour to a certain extent. A model to validate this concept is presented in this paper; this analytical model is based on typical material law behaviour hypotheses of beam nonlinear mechanical behaviour. The load–displacement and moment–curvature relationships predicted with this model were compared to the experimental results obtained for four large-scale specimens. The comparisons revealed good correlation between the analytical and experimental results and illustrate the potential of these composite beam configurations in civil engineering structures.

1. Introduction

In recent years, construction with ultra-high-performance short-fibre-reinforced concrete has increased significantly, both in Europe and worldwide. This material is strong in compression, more ductile in tension than plain concrete and can help mitigate the effects of environmental exposure because of its low permeability; thus, the industrial use of this material has increased, particularly when sustainable development principles are considered [1,2]. Use of this material enables a designer to create thinner sections and longer spans that are light, graceful and innovative in both geometry and form, with low permeability and good durability in terms of corrosion, abrasion and impact [3]. The material can be used without ordinary steel reinforcement (rebar). It requires less formwork, labour and maintenance than conventional concrete, therefore, reducing costs [4]. The elimination of shear stirrups enhances safety, reduces the weight of the structure and speeds construction. Its durability reduces maintenance requirements and extends service life. The use of UHPC in construction has significantly increased globally; consequently, new ways to optimise its use are now necessary [5,6].

In the past few years, the use of fibre-reinforced plastic (FRP) rebars to replace steel rebars has emerged as one of the numerous techniques proposed to enhance the corrosion resistance of reinforced concrete structures. In particular, FRP rebars offer significant potential for use in reinforced concrete construction when conventional steel-reinforced concrete has yielded unacceptable service [7–9]. The objective is to mix UHPC–SFR and FRP.

This paper presents the analytical and experimental results of an investigation of a new type of RC beam reinforced with UHPC–SFR.

The RC beams tested in this study were formed by casting FRP rebars in the bottom of an ultra-high-performance short-fibre-reinforced concrete (UHPC–SFR) beam, as shown in Fig. 1. The high-performance concrete, which has a minimum compressive strength of 150 MPa and a minimum tensile strength of 15 MPa, was placed in moulds to obtain beams as lightweight as possible. The elastic modulus of the UHPC–SFR was approximately 50,000 MPa [1,2]. The UHPC–SFR layers were internally reinforced with FRP bars to increase the tensile strength of the bottom portion of the RC beam [10].

* Corresponding author. Tel.: +33 04 72 69 21 21; fax: +33 04 78 94 69 06.
E-mail address: emmanuel.ferrier@univ-lyon1.fr (E. Ferrier).

http://dx.doi.org/10.1016/j.compositesb.2014.08.001
1359-8368/

Nomenclature

A_c	area of the UHP concrete (mm^2)
A_r	area of the rebars (mm^2)
A_w	area (mm^2)
b_w	width of the beam (mm)
d_c	depth of the concrete layer (mm)
d_r	depth of the rebars (mm)
$E_{1\%}$	initial Young's modulus of UHPC (MPa)
E_c	Young's modulus of UHPC (MPa)
E_{ci}	Young's modulus of layer i of the UHPC (MPa)
E_r	Young's modulus of the rebars (MPa)
F_c	force applied to the concrete (N)
f_{cc}	compressive strength (MPa)
f_{ct}	ultimate tensile strength of UHPC (MPa)
f_{ctj}	ultimate tensile elastic strength (MPa)
h	thickness of the laminate (mm)
h_{c1}	thickness of the lower plank (mm)
h_w	depth of the beam (mm)
l_c	UHPC crack length (mm)
M	applied moment (Nm)
m_c	internal bending moment in concrete (Nm)
m_{ext}	external bending moment (Nm)
m_r	internal bending moment in rebars (Nm)
M_u	ultimate bending moment (kN m)
m_w	internal bending moment in wood (Nm)
w_f	web thickness (mm)
V_u	ultimate shear load (kN)
z_g	neutral axis position (mm)
$\varepsilon(z)$	strain at depth z (m/m)
$\varepsilon_{0,3}$	elastic concrete strain in tension (m/m)
ε_{bc}	ultimate strain in UHPC (m/m)
ε_c	ultimate concrete strain (m/m)
ε_{cj}	concrete strain in layer j (m/m)
ε_{lim}	strain limit (m/m)
ε_r	strain in the rebars (m/m)
ε_{sup}	strain at the bottom of the beam (m/m)
$\varepsilon_w(i)$	strain in the concrete in layer i (m/m)
ρ_c	volume percentage of UHPC (%)
σ_c	compressive stress in concrete (MPa)
σ_r	rebar stress (MPa)
τ_w	maximum shear stress (MPa)
$w_{0,3}$	crack width of UHPC (mm)

Experimental testing was conducted on beams with 2- and 4-m spans. The high performance of this innovative RC structural configuration was demonstrated in this study.

An I-beam section was considered. The objective was to develop different failure modes. To accomplish this objective, the geometry of the section was adapted to each case study. The failure modes anticipated were tensile failure of the FRP reinforcement (in the beams with 4-m spans), compressive failure (in the beams with 4-m spans) and shear failure (in the beams with 2-m spans). The objective of the modelling conducted in this study was to use the typical analytical model developed for beams that includes concrete cracking and post-cracking behaviour to minimize material quantities by optimizing the UHPC thickness for shear and flexure and the FRP properties (rebar area and elastic modulus), thereby increasing the bending stiffness and ultimate load capacity.

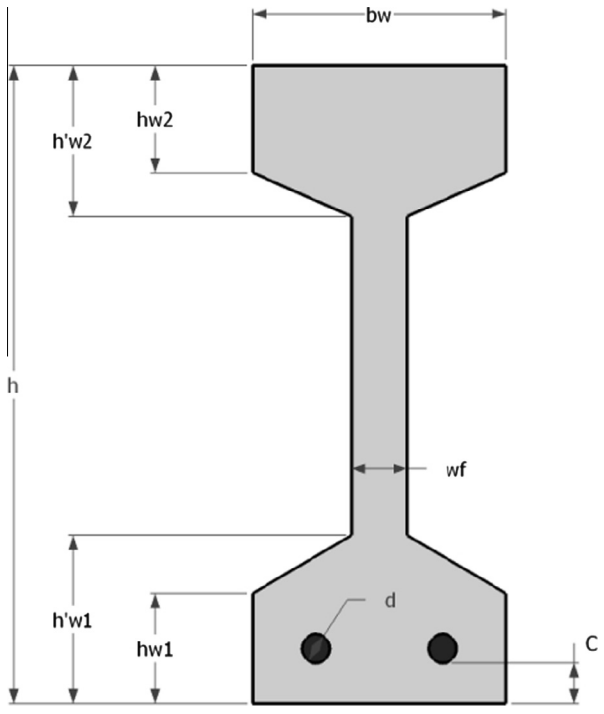

Fig. 1. Geometric parameters of beams.

2. Experimental program

2.1. Test specimens

A typical RC beam, similar to those described previously, is shown in Fig. 1. The length, width and height of a beam are denoted by L_w, b_w and h_w, respectively. The web thickness (w_f) is 22 mm for all beams because of the UHPC use (flow concrete with aggregate size less than 1 mm). The concrete cover of the FRP bars (c) is 15 mm. The thickness of the bottom flange of the beam reinforced with FRP is denoted by h_{w1}. The thickness of the top flange is denoted by h_{w2}. For comparison, the total depth was identical for each beam. Certain parameters were selected to evaluate the efficiency of the beams. Geometric and material parameters, such as beam length, depth and span, depth-to-width ratio, volume percentage of concrete versus short steel fibres, volume ratio of tensile rebar and rebar mechanical properties, including axial stiffness, and mechanical properties of concrete and FRP are all significant. The beam span, depth-to-width ratio and tensile strength of the rebars in the lower flange (Fig. 1) are the parameters investigated in this study. To test a full-scale specimen for building applications, a four-meter span was considered; shorter spans were also considered to study the shear limit of these beams. Four beams were designed for this study (Fig. 2). The geometric properties of the four beams studied are given in Table 2. For the four beams, the volume percentage of short metallic fibres was 2%, and the rebar axial stiffness E_rA_r was 20 and 30 MN for the carbon FRP rebars and 9 and 18 MN for the glass FRP rebars. The geometric and mechanical material properties of the glass (G) or carbon (C) fibre-reinforced polymer rebars are given in Tables 1 and 2. The depth-to-width ratios h/b_w were fixed in the range of 8–9.7 to produce the desired failure modes. The beam span-to-depth ratio L_w/h_w was nine for the four 2-m beams to produce shear failure and 20–22 for the four 4-m beams to produce flexural failure. The

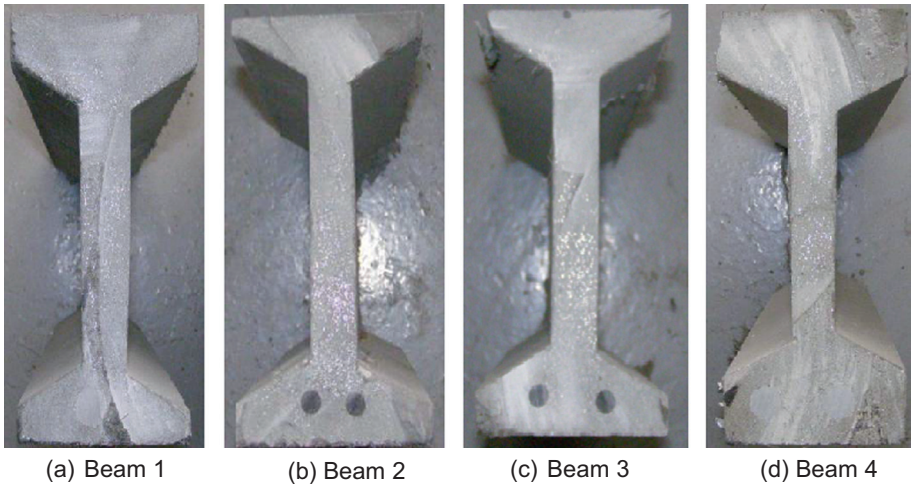

Fig. 2. Beams during testing.

Table 1
Parameters of mechanical behaviour laws.

Material		Parameter	Value	Units
Ultra-high-performance concrete	Tension	f_{ctj}	9	(MPa)
		ε_e	0.02	(%)
		f_{ct}	17	(MPa)
		$\varepsilon_{0.3\%}$	0.3	(%)
		$\varepsilon_{1\%}$	1	(%)
		ε_{lim}	10	(%)
	Compression	ε_{bc}	0.3	(%)
		f_{cc}	174	(MPa)
	Young's modulus	E_c	50,000	(MPa)
CFRP rebars	Tension	f_{FRPr}	1890	(MPa)
		ε_{re}	1.35	(%)
	Young's Modulus	E_r	140,000	(MPa)
GFRP rebars	Tension	f_{FRPr}	560	(MPa)
		ε_{re}	1.4	(%)
	Young's Modulus	E_r	40	(MPa)

Table 2
Materials and geometric properties.

	h_{w1} (mm)	h'_{w1} (mm)	h_{w2} (mm)	h'_{w2} (mm)	b_w (mm)	b_f (mm)	h_w (mm)	FRP TYPE CF/GF	Diameter (mm)	Number (u.)	Area (mm^2)
Beam 1	23	40	32	48	90	22	200	Glass	16	1	201
Beam 2	17	33	10	21	90	22	176	Carbon	9.6	3	217
Beam 3	17	33	10	21	90	22	192	Carbon	9.6	2	144
Beam 4	38	55	35	50	90	22	215	Glass	16	2	402

highest value for this ratio is expected to favour flexural behaviour rather than shear behaviour, which is more likely to control the shorter beams. The short-span beam 5 was lightened by a 50-mm diagonal void at 100-mm intervals in the flange (Fig. 2e).

2.2. Materials

As described above, the RC beams were constructed of an ultra-high-performance concrete. The UHPC was a Ductal® F1 premix. To evaluate its mechanical properties, mechanical tests were performed on each concrete batch. The four beams were cast in two different batches. Nine UHPC prisms were subjected to four-point bending tests to measure their modulus of elasticity E_c (Table 1). Nine cylindrical concrete specimens were tested in compression 90 days after casting, in accordance with the UHPC standard [11,12]. A mean compressive strength f_c of 174 ± 7.4 MPa was obtained. The material properties of the FRP rebars were not tested in the laboratory; the property values provided by the suppliers were used in the calculations (Table 1).

2.3. Specimen preparation

The FRP–concrete composite beams used in this study were fabricated by casting, as previously described. The FRP rebars were fixed in the mould because of their low density. The beams were cast horizontally from bottom to the top. The FRP bars were straight at their ends and no specific anchorage was placed. The tensile force in the FRP was obtained only in terms of bonding properties.

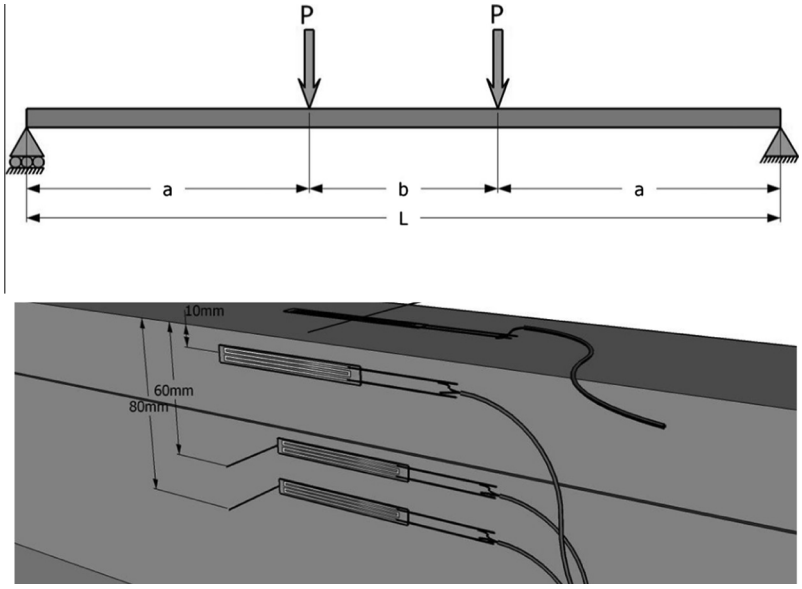

Fig. 3. Test configuration and strain gauge locations.

2.4. Mechanical testing

The tests conducted to determine the bending stiffnesses and load bearing capacities of the composite beams and their moment–curvature relations are illustrated in Fig. 3. The beam specimens, constructed as described above, were subjected to four-point bending tests. The distance between the supports and the applied load was greater than twice the depth of the beam. For the 2-m beams, this distance was 0.7 m (a value on Fig. 3); for the 4-m beams, it was 1.3 m (a value on Fig. 3). The distance between forces (b value on Fig. 3) was 0.6 m and 1.4 m for the 2-m beams and 4-m beams, respectively. The test was conducted under displacement control. The loads and displacements were measured at one-second intervals using load cells and LVDT transducers and recorded using a data logger. To obtain the strain distribution in the mid-span section, four strain gauges were bonded to the lateral faces of the beams. The rebar strains were also measured during loading, using gauges bonded to the rebars before the beams were cast. Before the tests, the beams were conditioned for at least 28 days to mean values of approximately 12% for moisture content and 20 °C for temperature.

3. Experimental results

3.1. Load–deflection response of composite beams

Analysis of the load–displacement curves indicated that there were two or three stages of distinct behaviour during the tests, corresponding to progressive damage in the constituent materials (concrete and rebars). The load–displacement curves for the three 4-m beams are shown in Fig. 4a, and those for the two 2-m beams are shown in Fig. 4b. For all beams with UHPC reinforced with GFRP or CFRP, the first stage of behaviour corresponds to that of the uncracked section. During this stage, the beams exhibited high bending stiffness. The second stage of behaviour began when the load reached approximately 11 kN for the 2-m-span beams and approximately 5 kN for the 4-m-span beams. In this stage, the concrete in the bottom flange of the beam began to crack, and a reduction in the bending stiffness was observed. This behaviour is consistent with the typical reinforced concrete beam mechanical response. The behaviour of the composite beam remains linear but with reduced bending stiffness until the third stage of behaviour (for beam 1), which corresponded to the yielding of short steel fibres at a load of approximately 35 kN for beam 1. After the cracking load, the behaviour remained elastic with constant stiffness until failure. This behaviour highlights the advantage of using FRP rebars to increase the tensile capacity of the beam because of the ultimate strength of the FRP, resulting in an increase in the ultimate capacity of the beam (Table 3).

3.2. Strain distribution in the section at mid-span

Based on the experimental strain measurements, strain as a function of measurement location (depth of the beam) is plotted for several loading levels to obtain the strain distribution in the middle section of the beam. The tensile strain on rebars provides the curve minimum values. Fig. 5 shows the evolution of strain in the central section of a beam at different load levels. The lower strain values on the FRP bars are obtained using the strain gauges. The results for the RC beams with carbon or glass FRP rebars are shown. The strains are planar and remain planar throughout loading in the compressive part and a small change in slope occurs in the bottom part. The linearity of the strain profiles confirms that no slip occurred at the interfaces between the FRP bars and the UHPC in this section. This observation also confirms the results previously obtained by Davalos et al. [13], Won et al. [14], Yang et al. [15] and Baena et al. [16], who conducted pullout tests and observed that use of high strength concrete with FRP results in high shear strength and perfect bonding can be assumed. For example, according to Mazahiripour et al. [17], using 10 mm FRP bars and an anchorage length of ten times the diameter, a 20 MPa concrete shear strength can be achieved in UHPC.

Splitting failure never occurred because fibre reinforcement mechanisms prevented the degeneration of microcracks into macrocracks [18].

The planar sections remain planar to failure. Some slip may occur at the end of the FRP bars near the support; however, the effect on the global behaviour of the beam and section equilibrium can be neglected. The bonding between the UHPC and the FRP rebars maintains strain continuity through the full height of the section, which confirms the reliability of this composite beam configuration. This was observed for all tested specimens. This result

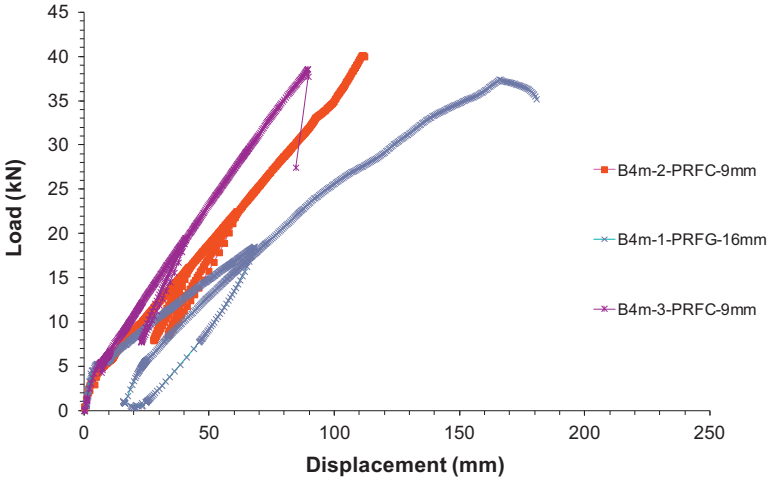

(a) Beams 1 to 3

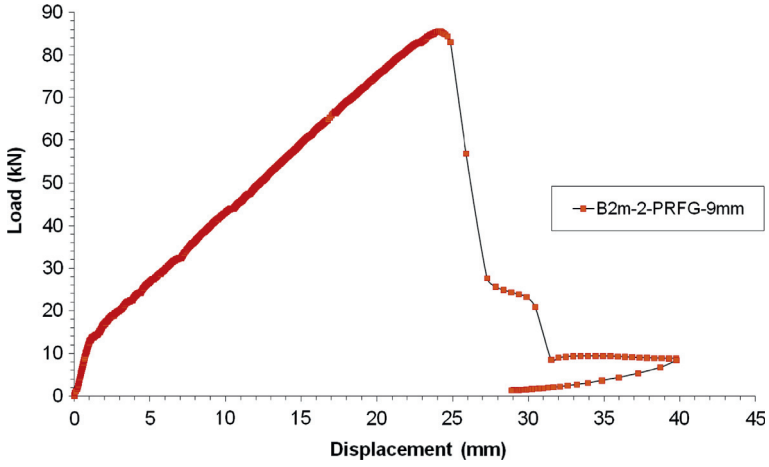

(b) Beams 4 and 5

Fig. 4. Load–displacement curves.

Table 3
Experimental results.

			Elastic limit load (kN)	Displacement at elastic load (mm)	Load at failure (kN)	Displacement at failure (mm)
Beam	1	B4-m-1-PRFG-16-mm	5.20	5.29	37.42	166
Beam	2	B4-m-3-PRFC-9-mm	5.50	5.12	38.62	90
Beam	3	B4-m-2-PRFC-9-mm	4.57	3.21	40.15	112
Beam	4	B2-m-2-PRFG-16-mm	13.62	1.20	85.55	24.13

confirms that the Navier and Bernoulli hypotheses of the mechanical behaviour of beams are satisfied and are useful for modelling.

Strain diagrams can be used to calculate the beam curvature for every load value and to measure the displacement of the neutral axis from its original position. Before cracking, the neutral axis is located at the mid-depth of the beam (Fig. 6). As cracking progresses, the neutral axis moves upward and stabilises at a height of approximately 70% of the total beam height, as measured from the bottom of the beam.

3.3. Behaviour at failure

Using the mid-section strain measurements (Table 4), the mechanical behaviour of the composite beams and the efficiency of the RC solution at failure can be evaluated. For the upper UHPC section in compression, the strain rate at failure was greater than 2500 μm/m for beam 3 (Fig. 7b) and nearly 2300 μm/m for beam 1 (Fig. 7a). For the FRP rebars, the maximum strength was attained in beam 1 with GFRP bars, whereas 80% of the CFRP strength was reached at failure for beam 3. For the 2-m beams, the tensile stress in the CFRP or GFRP varied from 20% to 50% of the maximum FRP strength because of the premature shear failure of the beam (Fig. 7c and Table 4). The beam design allows each material in the concrete to reach a high strain at failure in compression, confirming the benefits of this approach.

At the maximum load level, various failure modes were observed, depending on the span and characteristics of the beam. The 2-m beams failed in shear, whereas the 4-m beams exhibited compressive or tensile failure (Fig. 7). This confirms that for a L_w/h_w ratio of approximately ten, the design for shear should be

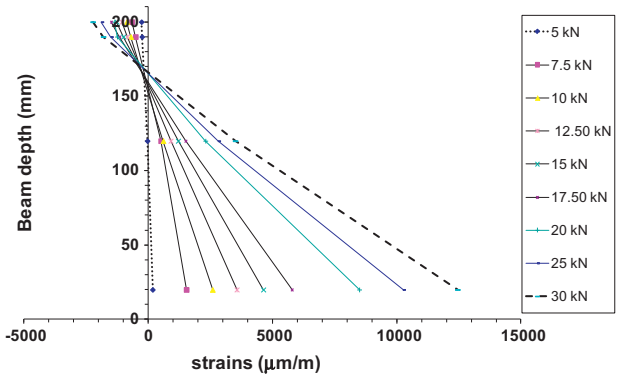

(a) B4-m-1-PRFG-16-mm

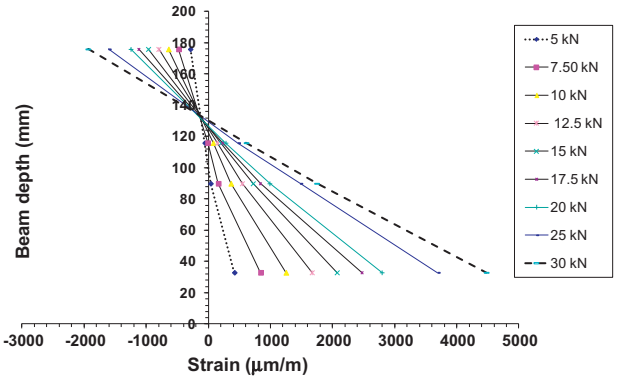

(b) B4-m-3-PRFC-9-mm

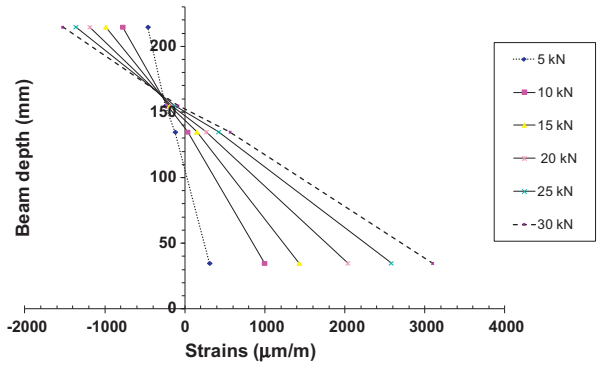

(c) B2-m-2-PRFG-16-mm

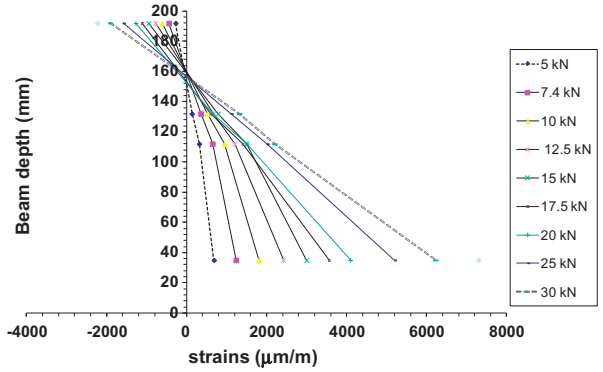

(d) B4-m-2-PRFC-9-mm

Fig. 5. Navier diagrams of beams 1–4.

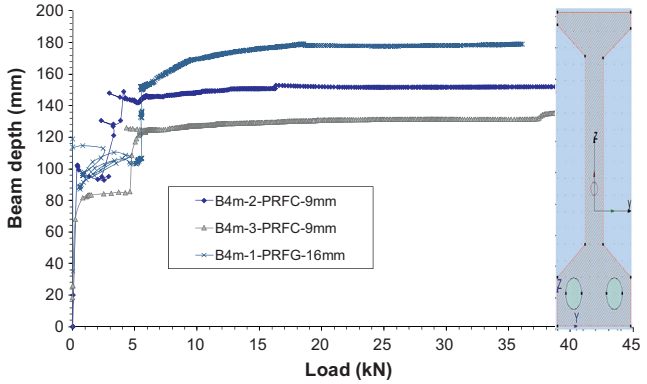

Fig. 6. Depth of neutral axis as a function of load.

carefully investigated and the width of the section increased to avoid shear failure. When the L_w/h_w value is approximately 20, the tensile or crushing failure are the critical design criteria if the width of the beam is large enough; however, in this study, the 22 mm flange thickness was sufficient. The failure of the RC beams occurred between loads of 37.4 (for beam 1) and 85 kN (for beam 4, 2-m span) (Table 3). There was no debonding of the FRP rebars from the UHPC in any of the beams, unlike FRP bars embedded in standard concrete [19,20]. The use of carbon composite rebars appears to be the most appropriate option for reducing span displacement because the Young's modulus of carbon FRP is higher than that of GFRP (Table 1). From these results, it was concluded that these new innovative RC beams allow UHPC to support higher stress at failure and that compressive strength of UHPC tensile failure of FRP can be obtained depending on the design, which improves the high performance material used.

4. Analytical modelling

Several authors have developed analytical methods to predict the loading capacity and fracture resistance of FRP-reinforced concrete flexural beams. For example, the constitutive law of FRP rods and the responses of plain concrete under appropriate tensile and compressive stresses were incorporated into the model developed by Wu et al. [21]. In this study, an analytical nonlinear material model of RC beams was used in an identical approach. A sectional analysis was initially used to develop an appropriate moment–curvature relationship for the composite sections. This numerical method is based on the Euler–Bernoulli beam theory combined with the layered approach. This modelling is well known in structural modelling to obtain the moment–curvature curve and the basic section equilibrium, and it was used in this paper. The analytical nonlinear material model was preferred to finite element analysis because of concrete cracking, the modelling of which would require a large number of elements to reduce the numerical instabilities caused by the size of the finite element mesh in a full 3-D analysis [22]. The method used in this study to predict the strength and stiffness of the multi-material RC beam is based on an iterative procedure, considering the mechanical properties of UHPC in compression and tension and FRP linear elastic behaviour. This analytical model, based on strain compatibility and equilibrium of internal forces in the section, can simulate the behaviour of the multi-material beam and include the nonlinearity of the constituent materials [23]. The causes of the nonlinearity of the section include tensile cracking of the concrete and reinforcement, plastic behaviour of the concrete in compression and yielding of the

Table 4
Values of maximum strain in UHPC and FRP bars.

			Top-of-beam maximum compressive strain (μm/m)	Maximum strain in FRP bars (μm/m)
Beam	1	B4-m-1-PRFG-16-mm	−2330	15,696
Beam	2	B4-m-3-PRFC-9-mm	−2417	6032
Beam	3	B4-m-2-PRFC-9-mm	−2585	8374
Beam	4	B2-m-2-PRFG-9-mm	−1459	7046

(a) Beam 1

(b) Beam 2

(c) Beam 4

Fig. 7. Failure modes.

internal short metallic reinforcement fibres. The contribution of short metallic fibres in tension embedded in UHPC should be considered. The analytical method allows the calculation of the deflection but does not consider the deflection increase from the shear contribution. This is generally neglected for RC structures but may explain the small differences observed for short span beams.

4.1. Material properties

UHPC–SFR has been thoroughly studied in tension, and several mechanical laws are available from these studies. Park et al. [24] confirmed the properties of UHPC–SFR internally reinforced by short metallic fibres. An elastic, multilinear stress–strain relationship proposed by Habel et al. [25] and AFGC [3] for UHPC–SFR was used to model the mechanical behaviour of the UHPC–SFR concrete. For concrete, the strain values corresponding to critical levels on the stress–strain curve are shown in Table 1 and are determined by the equations below. The tensile stress corresponding to initial cracking is f_{ctj}, with a strain value given by $\varepsilon_{0.3\%}$. The maximum point of the tensile stress–strain relationship is defined by the stress corresponding to f_{ct} and the strain corresponding to $\varepsilon_{1\%}$.

$$\varepsilon_{0.3} = \frac{w_{0.3}}{l_c} + \frac{f_{c_{tj}}}{E_{cj}} \tag{1}$$

$$\varepsilon_{1\%} = \frac{0.01h}{\frac{2}{3}h} + \frac{f_{c_{tj}}}{E_{cj}} \tag{2}$$

$$\varepsilon_{\lim} = \frac{15}{4h} + \frac{f_{c_{tj}}}{E_{cj}} \tag{3}$$

In these equations, h is the depth of the section, f_{ctj} is the ultimate tensile elastic strength, f_{ct} is the ultimate tensile strength of UHPC and E_{cj} is the elastic modulus of UHPC. Failure is assumed to occur in tension in UHPC when higher section strains in the tensile part reach the value of $\varepsilon_{\lim}$. When the concrete strain is greater than $\varepsilon_{\lim}$, the tensile stress is equal to zero.

This assumption can be made for the cracking behaviour of concrete internally reinforced by short metallic fibres [3].

Fig. 8(b) shows the linearly elastic stress–strain relationship for the CFRP or GFRP. Table 1 and Fig. 8(a) provide the parameter values of the mechanical behaviour laws for the UHPC and FRP materials.

4.2. Calculation procedure

This section details the established section calculation process for a multi-material beam analysis. The detailed calculation process is completed to analyse the specific materials used in this study. The stress–strain relationships for UHPC and the FRP reinforcements are combined with the section and span information to obtain the load–deflection and moment–curvature relationships of the beam [23]. Relevant data include the height and width of the beams, depth and amount of FRP reinforcement, geometries of the UHPC–SFR sections, and span lengths and positions of the external loads. To initiate the calculation procedure, the value of strain in the top concrete (ε_{sup}) and the depth of the neutral axis (z_g) are assigned arbitrarily. The depth of the beam is divided into 200 slices. The strain profile along the height of the beam is obtained from the following equations, based on the assumption that the planar section remains planar:

$$\varepsilon_c(i) = \frac{(d_c(i) - z_g)}{d_c(i)}\varepsilon_{sup} \tag{4}$$

and

$$\varepsilon_r = \frac{(d_r - z_g)}{d_r}\varepsilon_{sup} \tag{5}$$

where $\varepsilon_c(i)$ is the strain in UHPC layer i, d_r is the depth of the rebars, and ε_r is the strain in the reinforcing bars (Fig. 9).

An average strain is calculated for each fibre, and the corresponding compressive and tensile stresses are determined using the stress–strain relationship for each material. The tensile concrete failure is given by a strain limit according to the material law definition ($\varepsilon_{\lim}$). When the concrete strain is greater than ($\varepsilon_{\lim}$), the tensile stress is equal to zero. In compression, UHPC exhibits elastic behaviour until the ultimate strength is reached. Compression post-peak behaviour is not considered in this study; therefore, according to material laws, concrete can be assumed to be elastic.

Multiplying the stress by the area of the fibre provides the compressive and tensile forces. The following equations are used for this purpose:

$$\sigma_c = \sum_{i=1}^{n} E_c\varepsilon_c(i) \tag{6}$$

$$F_c = \sum_{i=1}^{n} A_c(i)E_c\varepsilon_c(i) \tag{7}$$

$$\sigma_r = E_r\varepsilon_r \tag{8}$$

$$F_r = A_rE_r\varepsilon_r \tag{9}$$

where A_r is the area of the rebars and A_c is the area of the concrete section. After all forces are calculated, the equilibrium of the section is verified with the following equation:

$$\sum F = 0 = A_rE_r\varepsilon_r + \sum_{i=1}^{n} A_c(i)E_c\varepsilon_c(i) \tag{10}$$

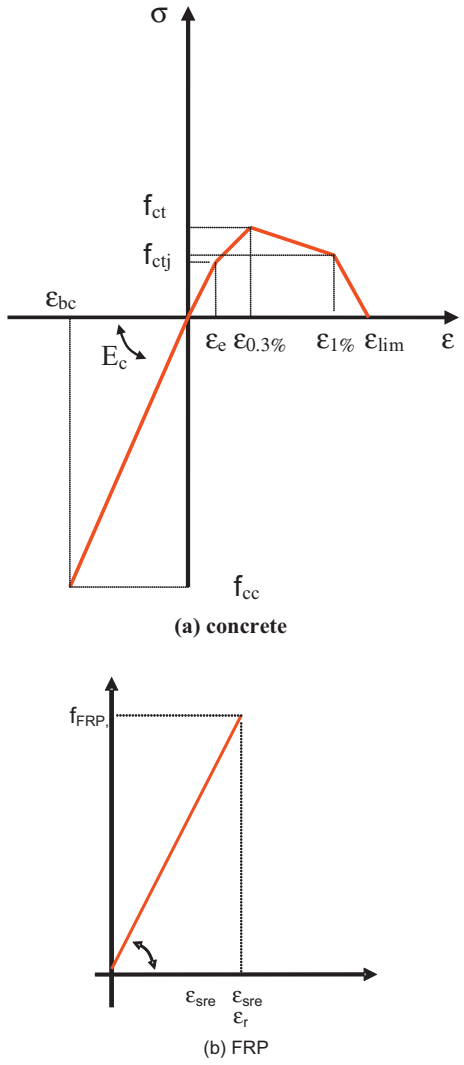

Fig. 8. Mechanical behaviour of materials.

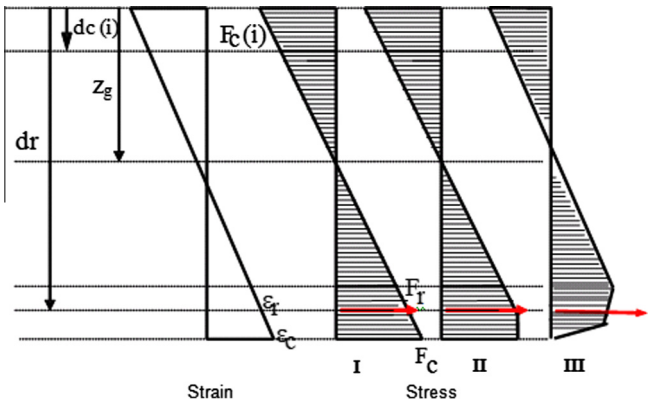

Fig. 9. Section equilibrium principle.

If equilibrium conditions are not satisfied, the position of the neutral axis (z_g) is then moved to a different location, and the process is repeated until the sum of the compressive forces in the section balances the sum of the tensile forces. Once the iterative procedure has converged to equilibrium, the internal moment and the curvature are determined by considering the load and location of the material splice (Eqs. (10)–(13)).

$$\sum m = m_{ext} = m_r + m_c \tag{11}$$

with

$$m_r = A_r E_r \varepsilon_r (d_r - z_g) \tag{12}$$

$$m_c = \sum_1^i A_c(i) E_c \varepsilon_c(i) (d_c(i) - z_g) \tag{13}$$

In determining the theoretical moment–curvature relationship for the composite section in flexure, it is assumed that planar sections remain planar and the longitudinal strain is directly proportional to the distance from the neutral axis.

A finite-difference method is used to calculate the deflection of the beam. Taking advantage of the symmetry of the loaded beam, the finite-difference calculation is performed with one-half of the beam that is divided into five sections. A flow chart of the calculation procedure is shown in Fig. 10. The computation is conducted in a Visual Basic environment. The moment–curvature and load–displacement curves are calculated, and at any level of loading, the strains and stresses in each constituent material can be determined (Fig. 11).

4.3. Failure criteria

The calculation continues by incrementing the applied load until the maximum strength of one of the materials is reached. The possible failure modes in compression that must be considered include the crushing of the topmost fibres in the UHPC–SFR. In tension, failure of the RC beam may occur in the FRP or in the bottommost fibre of the beam. Tensile failure of the concrete in the lower UHPC–SFR is also considered based on the UHPC equivalent mechanical law.

In a reinforced concrete beam, shear controls the design when the flange width is small. It is therefore necessary to check the shear strength. According to the AFGC standard [3], the maximum shear stress of a composite beam can be assessed as follows:

$$V_f \leqslant V_u \tag{14}$$

The horizontal shear stress at the neutral axis is given by the following equation:

$$V_f = \frac{S \cdot \sigma_p}{\gamma_{bf} \cdot \tan(\beta_u)} \tag{15}$$

where V_u is the applied shear force (N), σ_p is average post-crack residual tensile strength σ_P of UHPC (MPa), S is concrete shear area (mm^2), γ_{bf} is safety factor for concrete (equal to one here) and β_u is crack angle (equal to 45° in this study).

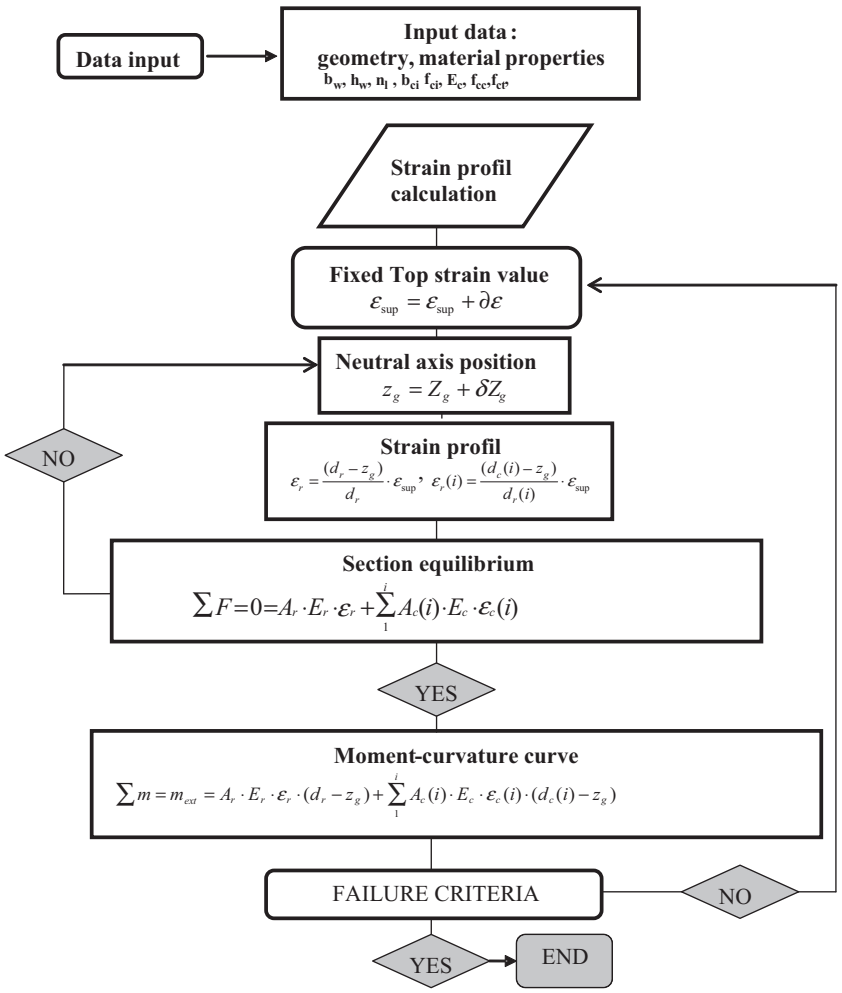

Fig. 10. Calculation procedure.

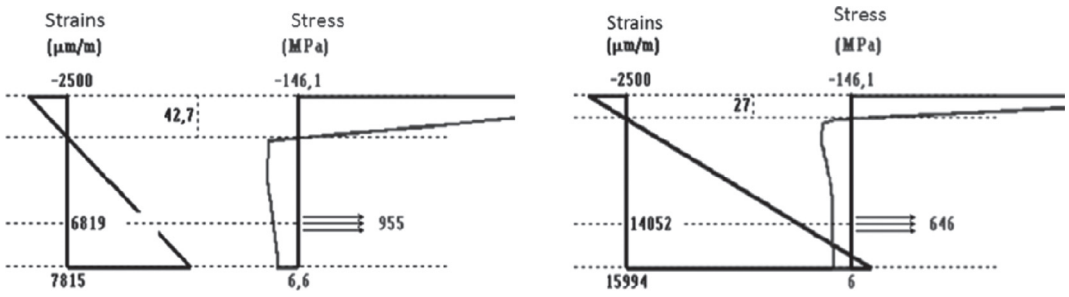

Fig. 11. Examples of resulting strain and stress profiles for B4-m2PRFC-9 mm.

This method allows for the calculation of the maximum shear stress in the beam and the comparison of this value to the UHPC shear strength [26–30]. Here, $S = b_0 z$ is the resistance area of the fibres, calculated by multiplying the width of the web b_0 by the lever arm z between the tensile and compressive resultant forces. It is assumed that $z = 0.9d$ for rectangular sections [4], which is a conservative assumption for T-sections. The parameter $ß_u$ represents the angle between the concrete compression struts and the neutral fibre of the beam. A partial safety factor γ_{bf} was introduced to account for any manufacturing defects that influence the tensile properties of the UHPC. The value of this partial safety factor was 1.3 for the case of fundamental combinations and 1.05 for the case of accidental combinations (but was equal to one in this study).

The average post-crack residual tensile strength σ_p can be calculated as follows:

$$\sigma_p = \frac{1}{K} \cdot \frac{1}{w_{\lim}} \int_0^{w_{\lim}} \sigma(w) dw \tag{16}$$

The value of variable σ_p is determined from the maximum design crack width $w_{\lim}$ and the stress-versus-crack width relationship $\sigma(w)$. A maximum design crack width of 0.3 mm is recommended in the French code. If it is assumed that the stress-versus-crack width relationship is linear up to the maximum crack width of 0.3 mm, then the value of σ_p can be estimated as the average of the stress level corresponding to a zero crack width, corresponding to a crack width of 0.3 mm. The anisotropy of the fibre orientation distribution is not considered ($K = 1$).

The results are summarised in Table 5 and are based on the following assumptions. The design safety factors γ_{bf} were set to 1.0, and angle $ß_u$ was assumed to be 45°. A linear stress-versus-crack width response was assumed for crack widths up to 0.3 mm. Therefore, the average post-crack strength can be estimated as $\sigma_p = 9$ MPa, based on the literature (Xia et al. [28]).

The shear strength prediction, based on the French code, at a maximum crack width of 0.3 mm was significantly lower (−25%) than the test results for beams 4 and 5, which indicates that the standard is conservative. The shear strength is underestimated because the predicted value actually corresponds to a shear crack width of 0.3 mm and the secondary contribution is not considered.

Table 5
Comparison of theoretical and experimental loads for shear.

	b_f (mm)	h_w (mm)	S (mm^2)	V_f (kN)	Vu_{exp} (kN)
Beam 1	22	200	3564	32.1	18.7
Beam 2	22	176	3136	28.2	19.3
Beam 3	22	192	3421	30.8	20.1
Beam 4	22	215	3831	34.5	42.8

4.4. Experimental/theoretical comparison

The results of the laboratory tests on the four RC beams were used to assess the validity of the analytical model (Fig. 12 and Table 6).

The load–displacement and moment–curvature curves obtained experimentally for the 2- and 4-m spans were compared to those developed using the analytical model.

In Fig. 12, the load–displacement relationship obtained from the analytical model is compared to the experimental results. The typical moment–curvature relationship can be idealised as nonlinear (Fig. 12). In the first portion of the curve, all materials remain elastic; the concrete starts to crack in tension during the second stage.

The experimental load–deflection curves exhibit two stages of identical behaviour predicted by analytical modelling. The theoretical and experimental curves are consistent. The stages of behaviour are well represented, and the slope of the curve is obtained with accuracy in excess of 95%.

Tables 5 and 6 compare the ultimate loads and displacements at failure and the predicted and observed failure modes. The prediction of the ultimate load is less accurate than that for the bending behaviour discussed in the previous section. For the 4-m span beams in which the predominant failure mode was tension or compression, the prediction of the ultimate load is satisfactory; the predicted values differed from the experimental values by approximately 7–17%. For beams with small dimensions, the predictions are also accurate, with predicted failure loads ranging from 0.96% to 1.18% of the experimental failure loads.

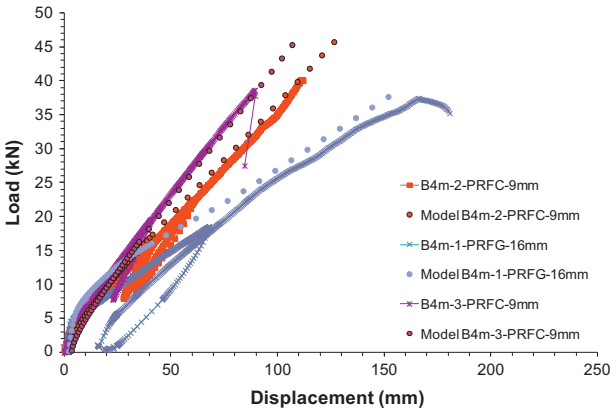

Fig. 12. Comparison of experimental and numerical results for load–displacement curves.

Table 6
Comparison of theoretical and experimental loads and displacements.

	Load at failure (kN)	Displacement at failure (mm)	Theoretical load at failure (kN)	Theoretical displacement at failure (mm)	Normalised load	Failure mode
Beam 1	37.42	166	39.8	176	1.06	FRP in tension
Beam 2	38.62	90	48.9	113	1.26	UHPC in compression
Beam 3	40.15	112	50.3	140	1.25	UHPC in compression

5. Parametric study

Based on the modelling, the effect of the FRP rebar ratio was estimated as a function of the ultimate bending moment criterion and the serviceability limit state. To evaluate the contributions of the various materials and geometries, an analytical method was used to investigate the 23 cases listed in Table 7. The case studies focused on flexural rigidity, assuming that beams do not fail in shear. The parameters studied were the volume ratio of the tensile reinforcement and its Young's modulus, the volume ratio of the UHPC–SFR and the depth of the beam. The volume ratio of the FRP bars ranged from 0.25% to 4%, and both carbon and glass FRP bars were considered [30]. A serviceability limit for mid-span deflection of 1/250 of the beam span was used, based on the value for steel and timber beams. The cross section in Fig. 1, with a total depth (H) of 200 mm, a span of 4 m (L) and a span-versus-depth ratio of 1/20, was studied. Another span-versus-depth ratio was considered to evaluate the effect of this ratio on both ultimate capacity and serviceability behaviour. The highest ratio value was expected to favour flexural behaviour rather than shear behaviour, which is more likely to affect shorter beams. Table 7 summarises the parameters used in this case study.

The FRP reinforcement ratio is given by Eq. (17) as follows:

$$\rho_f = \frac{A_r}{A_c} \tag{17}$$

where A_r is the cross-sectional area of the FRP bars and A_c is the cross-sectional area of the concrete.

The load–displacement curves in Figs. 14 and 15 illustrate the influence of the material properties and the effect of the relative size of the FRP bars on beam behaviour. As the area of the FRP bars as a proportion of the section area increases, the maximum load and displacement increase. The bending stiffness behaviour of the concrete can be investigated as a mechanism to control the beam behaviour.

The material properties of the rebar directly influence the ultimate behaviour of the beam. For instance, Fig 15 and Fig. 16 show the benefits of using CFRP rebar rather than GFRP. When CFRP rebar is used, the model predicts behaviour with less displacement and a higher bending stiffness.

The ratio between the ultimate bending moment and the serviceability limit state (a displacement limit of L/250) was examined as a function of the reinforcement ratio. The normalised equation is as follows:

Table 7
Parameters for case studies.

Case	FRP ratio (%)	Rebars	Young's modulus (GPa)	H/L
1	0.25	CFRP	140	20
2	0.50	CFRP	140	20
3	1	CFRP	140	20
4	1.5	CFRP	140	20
5	2	CFRP	140	20
6	3	CFRP	140	20
7	3.5	CFRP	140	20
8	4	CFRP	140	20
9	0.25	CFRP	140	15
10	0.50	CFRP	140	15
11	1	CFRP	140	15
12	1.5	CFRP	140	15
13	2	CFRP	140	15
14	3	CFRP	140	15
15	3.5	CFRP	140	15
16	4	CFRP	140	15
17	0.50	GFRP	40	20
18	1	GFRP	40	20
19	1.5	GFRP	40	20
20	2	GFRP	40	20
21	3	GFRP	40	20
22	3.5	GFRP	40	20
23	4	GFRP	40	20

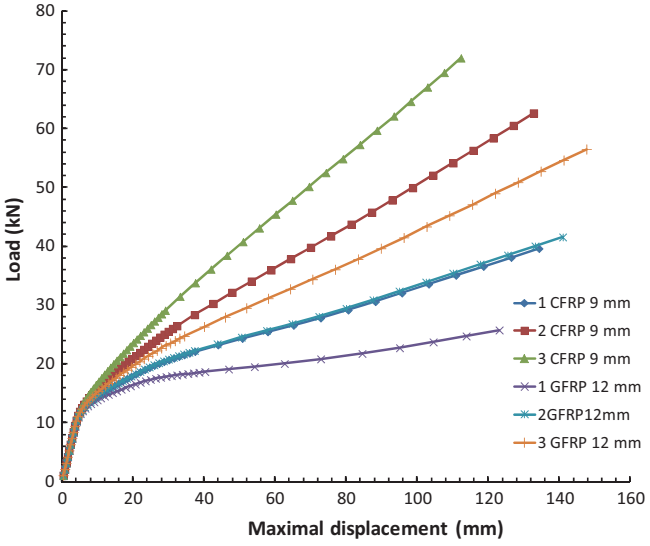

Fig. 13. Load–displacement response for different FRP ratios.

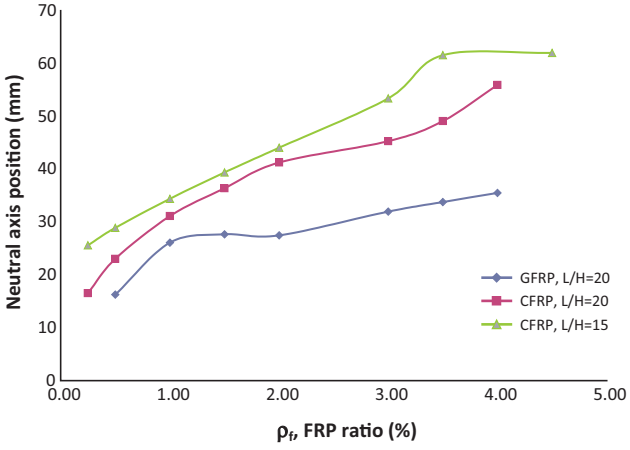

Fig. 14. Neutral axis position from top of the beam versus FRP ratio for $H/L = 20$.

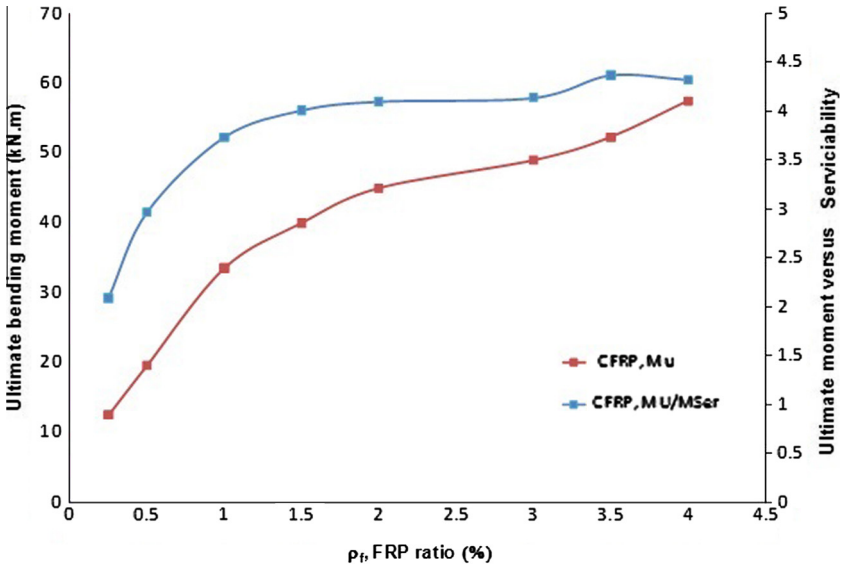

Fig. 15. Ultimate bending moment and serviceability ratio versus FRP ratio for $H/L = 15$.

$$\frac{M_u}{M_{ser}} = f(\rho_r) \tag{18}$$

The effect of the ultra-high-performance concrete volume, as a function of the FRP bar volume, on the rigidity of the member is shown in Fig. 13. A small amount of UHPC–SFR produces an increase in the initial bending stiffness and modifies the bending stiffness during loading.

The influence of the UHPC–SFR ratio on the moment (M)–curvature (φ) curve is illustrated in Fig. 13; by increasing the UHPC–SFR ratio, a transition from a brittle collapse (a linear M–φ relationship) to a ductile failure (a nonlinear M–φ relationship) is possible when a low ratio of FRP is used. The bending stiffness essentially depends on the axial stiffness of the rebar.

Fig. 14 shows the neutral axis position from the top of the beam at failure as a function of the FRP ratio and Young's modulus for two different span-to-depth ratios. As expected, higher FRP bar ratios result in lower neutral axis positions. This parameter must be considered for design purposes; in this case, it is calculated in terms of the tensile behaviour of concrete, providing a precise value.

Fig. 15 allows for the observation of the ultimate bending moment as a function of the FRP reinforcement ratio for a span length-to-depth ratio of 15; beyond the 2% FRP reinforcement ratio, the ultimate bending moment does not increase because the compressive failure mode is obtained. Therefore, the optimum value for RC beams made of UHPC–SFR and reinforced by FRP is 2% for a span-versus-depth ratio of 1/20.

If the product of the rebar area and Young's modulus remains constant, then the composite beam will possess the identical bending stiffness. The most influential property of FRP rebar is its ultimate strength, which allows an increase in the ultimate capacity of the beam up to the compressive strength of the concrete. Suitable rebar materials can be selected depending on the design requirements for bending strength or load-bearing capacity. The percentage of UHPC in the section primarily influences the ductility of the RC beam. For structural design purposes, the main design criterion will be related to the service condition (deflection criterion), similar to glulam or steel beams. The axial stiffness of the FRP rebars should be considered in their design.

6. Conclusions

This paper describes the development and testing of an innovative RC beam constructed of ultra-high-performance concrete and reinforced with short fibres and FRP reinforcing bars.

The results demonstrate the following:

- The beam exhibits typical RC beam behaviour in terms of concrete cracking and failure in tension or compression.
- The results indicate that reinforcing concrete with carbon FRP rebar increases the concrete bending stiffness, even with a small diameter rebar, by increasing its Young's modulus.
- Glass FRP bars can provide similar results, but a larger rebar area is required. The most influential parameter is the axial stiffness of the reinforcement.
- To analyse the cracking behaviour of the concrete in tension, an iterative calculation method was developed that provided the following conclusions:
- The moment–curvature and load–displacement relationships may be determined using this calculation method.
- The maximum bending capacity can be determined with high accuracy.
- The ultimate shear load is underestimated by this calculation method, which is conservative.

This study confirms that the composite action of high performance materials in an RC beam can result in a lightweight structure that is mechanically efficient. The results of this study should be confirmed by a more extensive experimental program using large-scale beams and a larger number of specimens. The fatigue and creep behaviour of the RC beam developed in this study should also be investigated.

References

[1] Yang In Hwan, Joh Changbin, Kim Byung-Suk. Structural behavior of ultra high perform ance concrete beams subjected to bending. Eng Struct 2010;32(11):3478–87.
[2] Behloul M et al. The Sherbrooke footbridge: the first reactive powder concrete structure. Struct Eng Int 1998:140–4.

[3] AFGC (Association Française de Genie Civil), Interim Recommendations Ultra-High performance, Fiber-Reinforced Concretes, AFGC Publication, France; January 2002.
[4] Acker P, Behloul M. Ductal® technology: a large spectrum of properties, a wide range of applications. Avignon, France: FIB symposium; 2004.
[5] Perry V, Royce M. Innovative field-cast UHPC joints for precast bridge decks (side-by-side deck bulb-tees), Village of Lyons, NY – Design, Protoyping Testing and Construction, Concrete Bridge Conference, USA; 2007.
[6] Akhnoukh Amin Kamal, Xie H. Welded wire reinforcement versus random steel fibers in precast/prestressed ultra-high performance concrete I-girders. Constr Build Mater 2010;24(11):2200–7.
[7] Chaallal O, Benmokrane B. Fiber-reinforced plastic rebars for concrete applications. Compos B Eng 1996;27(3–4):245–52.
[8] Tighiouart B, Benmokrane B, Gao D. Investigation of bond in concrete member with fibre reinforced polymer (FRP) bars. Constr Build Mater 1998;12(8):453–62.
[9] Benmokrane B, Chaallal O, Masmoudi R. Glass fibre reinforced plastic (GFRP) rebars for concrete structures. Constr Build Mater 1995;9(6):353–64.
[10] El-Hacha R, Chen D. Behavior of hybrid FRP–UHPC beams subjected to static flexural loading. Compos B Eng 2012;43(2):582–93.
[11] Japan Society of Civil Engineers, Recommendations for design and construction of ultra-high strength fiber reinforced concrete structures; September 2006.
[12] U.S. Dept. of Transportation - Federal Highways Administration, Material Property Characterization of Ultra-High Performance Concrete Prestressed I-Girders, (Publication No. FHWA-HRT-06-103), August; 2006.
[13] Davalos JF, Chen Y, Ray I. Effect of FRP bar degradation on interface bond with high strength concrete. Cement Concr Compos 2008;30:722–30.
[14] Won Jong-Pil, Park Chan-Gi, Kim Hwang-Hee, Lee Sang-Woo, Jang Chang-Il. Effect of fibers on the bonds between FRP reinforcing bars and high-strength concrete. Compos B Eng 2008;39(5):747–55.
[15] Yang Jun-Mo, Min Kyung-Hwan, Shin Hyun-Oh, Yoon Young-Soo. Effect of steel and synthetic fibers on flexural behavior of high-strength concrete beams reinforced with FRP bars. Compos B Eng 2012;43(3):1077–86.
[16] Baena Marta, Torres Lluís, Turon Albert, Barris Cristina. Experimental study of bond behaviour between concrete and FRP bars using a pull-out test. Compos B Eng 2009;40(8):784–97.
[17] Mazaheripour H, Barros JAO, Sena-Cruz JM, Pepe M, Martinelli E. Experimental study on bond performance of GFRP bars in self-compacting steel fiber reinforced. Compos Struct 2013;95(January):202–12.
[18] Pepe M, Mazaheripour H, Barros J, Sena-Cruz J, Martinelli E. Numerical calibration of bond law for GFRP bars embedded in steel fibre-reinforced self-compacting. Compos B Eng 2013;50(July):403–12.
[19] Wu ZJ, Ye JQ. Strength and fracture resistance of FRP reinforced concrete flexural members. Cement Concr Compos 2003;25:253–61.
[20] Bakis CE, Uppuluri VS, Nanni A, Boothby TE. Analysis of bonding mechanisms of smooth and lugged FRP rods embedded in concrete. Compos Sci Technol 1998;58(8):1307–19.
[21] Wu ZJ, Ye JQ. Strength and fracture resistance of FRP renoforced concrete flexural members. Cement Concr Compos 2003;25:253–61.
[22] Ranzi G, Bradford MA. Direct stiffness analysis of a composite beam–column element with partial interaction. Comput Struct 2007;85(15-16):1206–14.
[23] Kwak Hyo-Gyoung, Kim Sun-Pil. Nonlinear analysis of rc beams based on moment-curvature relation. Comput Struct 2002;80:615–28.
[24] Park Seung Hun, Kim Dong Joo, Ryo Gum Sung. Tensile behavior of ultra high performance concrete. Cem Concr Compos 2012;34(2):210–8.
[25] Habel K, Viviani M, Denarié E, Brühwiler E. Development of the mechanical properties of an ultra-high performance fiber reinforced concrete (UHPFRC). Cem Concr Res 2006;36(7):1362–70.
[26] El-Hacha R, Abdelazeem H, Cariaga I. Effect of casting method and shear span-to-depth ratio on the behavior of Ultra-High Performance Concrete cross arms for high voltage transmission lines. Eng Struct 2010;32(8):2210–20.
[27] Chen D, El-Hacha R. Damage tolerance and residual strength of hybrid FRP–UHPC beam. Eng Struct April 2013;49:275–83.
[28] Kang Su-Tae, Lee Yun, Park Yon-Dong, Kim Jin-Keun. Tensile fracture properties of an Ultra-high-performance Fiber Reinforced Concrete (UHPFRC) with steel fiber. Compos Struct 2010;92(1):61–71.
[29] Xia J, Mackie KR, Saleem MA, Mirmiran A. Shear failure analysis on ultra-high performance beams reinforced with concrete high strength steel. Eng Struct 2011;33(12):3597–609.
[30] Lau Denvid, Pam Hoat Joen. Experimental study of hybrid FRP reinforced concrete beams. Eng Struct 2010;32(12):3857–65.